NEUROIMAGE **4,** S76–S83 (1996)
ARTICLE NO. 0057

Functional Magnetic Resonance Neuroimaging Data Acquisition Techniques

JEFF H. DUYN,[1] YIHONG YANG, JOSEPH A. FRANK, VENKATA S. MATTAY, AND LEI HOU

Functional MRI studies of human brain require rapid data acquisition techniques, to map dynamic changes with sufficient anatomical coverage. In addition, task activation studies employing functional MRI require a high scan sensitivity, in order to discriminate the small, activation-related signal changes from background noise. An overview is given of current fast scan methods, which are sensitized to detect susceptibility changes related to task-induced changes in blood oxygenation. Sources of artifacts are discussed, as well as their effect on image quality. © 1996 Academic Press, Inc.

INTRODUCTION

In addition to mapping of brain anatomy, MRI can be applied to the study of brain function. Tissue perfusion can be assessed with magnetic labeling of arterial spins [1] or the intravenous bolus injection of paramagnetic contrast agents [2]. Recently it has been demonstrated that MRI can also indirectly detect changes in brain activity with task activation studies, either by employing exogenous contrast agents [3] or by measuring changes in blood oxygenation level [4, 5].

An important aspect of functional MRI (fMRI) studies employing blood oxygenation dependent (or BOLD) contrast is the noninvasive character, and the relatively short acquisition times, allowing for multiple repetitions to be performed on a single subject. However, some questions remain unanswered, in particular those with regard to what contrast mechanisms have contributions to the signal changes observed in BOLD fMRI, and what is the optimal data acquisition technique. In the following, an overview of current acquisition techniques is presented, and potential contrast mechanisms are discussed.

MRI DATA ACQUISITION

In MRI, signal is generated by exciting the proton spins with radio-frequency (RF) irradiation (Fig. 1). This causes the magnetization to tilt away from the main field direction (longitudinal direction) by an angle equal to the excitation angle (also called flip angle), and results in the creation of transverse magnetization components. In an idealized experiment with perfectly uniform magnetic field, the transverse magnetization starts to precess at the Larmor frequency, generating a signal with a phase increasing over time. Localization is achieved by the use of magnetic field gradients [6] (Fig. 1), which induce additional phase accumulations (modulations) of the signal. The phase evolution for each proton spin is now dependent on its location in combination with the strength and direction of the applied field gradient (hereafter called localization gradient), and the signal is generally composed of many components with different frequencies (phase evolutions). After phase-sensitive detection during a readout window T_{acq} (Fig. 1), the signal is digitized and saved in a raw data array. Together with the information concerning the pulsed gradient (gradient wave from), this data array constitutes the so called k-space data [7, 8]. To collect a single two-dimensional (2D) image, an entire plane (2D-array) in k-space needs to be collected. This generally requires multiple repetitions of the pulse sequence, while altering the wave forms of the localizing gradient. As final step, the MR image is reconstructed by Fourier analysis of the raw data (k-space data).

For an fMRI experiment, multiple images are acquired sequentially over time, during the execution of a task activation paradigm. Several image processing steps are needed to extract activated brain areas from the time series data. These steps include image registration, subtraction of images acquired during rest stages from images acquired during active stages, statistical significance tests, and overlay on anatomical images.

IMAGE ARTIFACTS

Artifacts in MRI can have various origins. Most artifacts arise when the phase and amplitude of the MR signal are affected by sources other than the localization gradients. These sources include regional differences in magnetic susceptibility (e.g., at air–tissue interfaces), chemical shift (e.g., protons in lipid), transverse relaxation (exponential signal decay over time, indicated by decay time constant T_2), as well as subject (or tissue) motion and scanner instabilities. Any of

[1] To whom correspondence should be addressed at the Laboratory of Diagnostic Radiology Research, OIR, NIH, Building 10, Room B1N-256, Bethesda, Maryland 20892. Fax: (301) 402-3216; E-mail: jhd@helix.nih.gov.

1053-8119/96 $18.00
Copyright © 1996 by Academic Press, Inc.
All rights of reproduction in any form reserved.

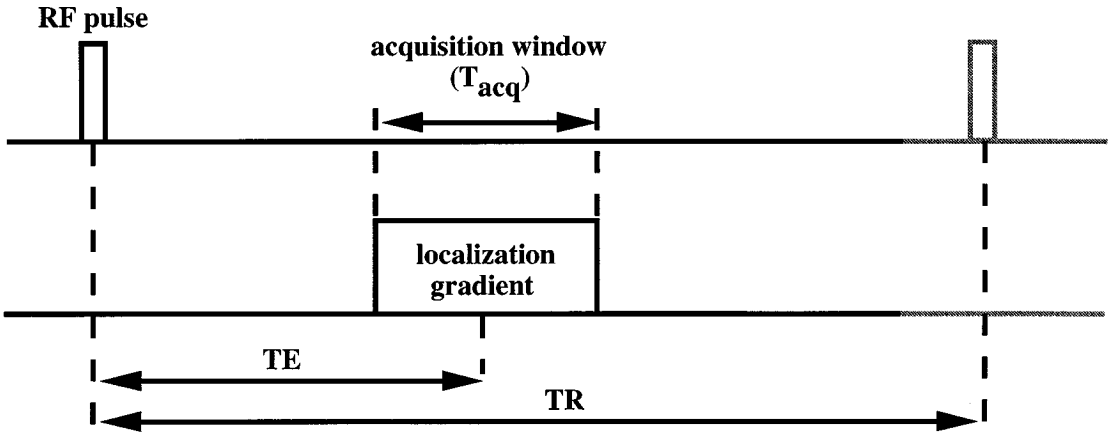

FIG. 1. Basic MR pulse sequence, showing timing of RF and gradients. MR signal is generated using an RF excitation pulse, and measured at time T_E during the readout window (T_{acq}). Localization is performed during T_{acq} using a magnetic field gradient. The sequence is repeated after a repetition time T_R.

these sources can cause signal fluctuations during the readout window, which are, except for those caused by motion and scanner instabilities, identical for each repetition. The severity of artifacts is related to the duration of the acquisition window T_{acq} (Fig. 1), and, in the case of motion, to the duration of the entire experiment (i.e., T_R times the number of repetitions needed to collect the k-space data). In all cases, the contribution of artifacts is strongly dependent on acquisition technique and parameters.

SINGLE-SHOT MRI

Single-shot MRI techniques aim at collecting the entire k-space data array in a single repetition of the pulse sequence. Examples are echo planar imaging (EPI) [9–11] and spiral imaging [7, 12]. An important advantage of single-shot techniques is their short scan time, and with it their relative insensitivity to motion artifacts. This advantage has helped to make single-shot imaging an important technique for fMRI. Figure 2 shows an example of results of a motor cortex activation study obtained with single-shot spiral fMRI on a normal subject.

Both EPI and spiral techniques require extensive switching of the direction and amplitude of the localization gradient within the acquisition time, and pose high demands on gradient hardware. Until recently, single-shot imaging was only feasible on dedicated MRI scanners, or scanners equipped with insertable head-

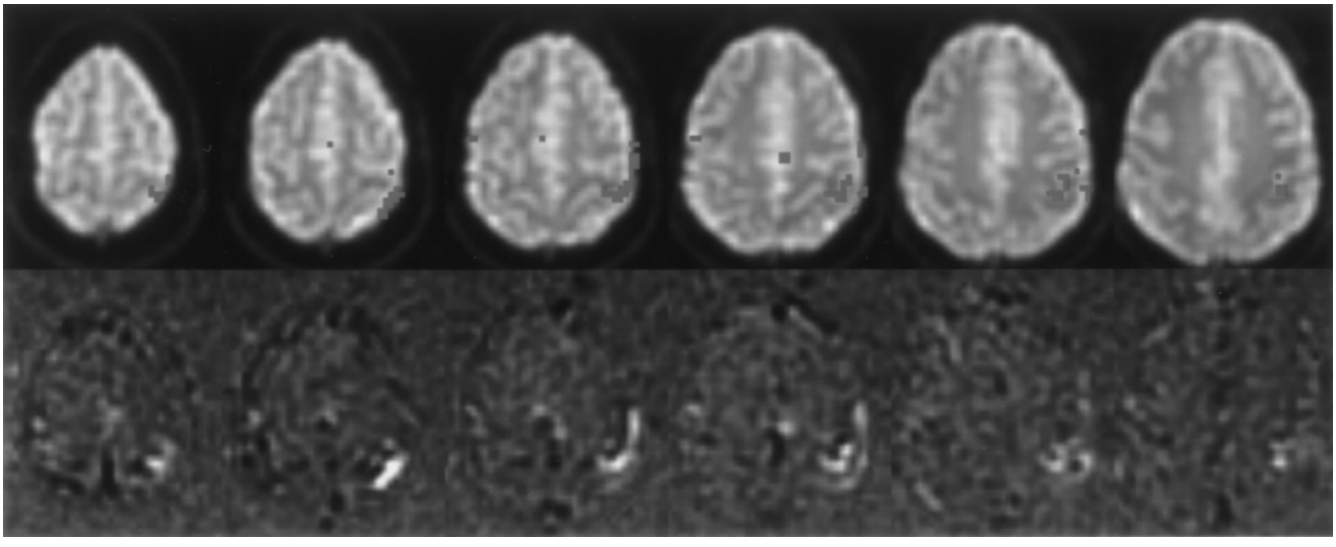

FIG. 2. Motor cortex activation experiment using a 36-slice single-shot spiral technique (a subset of 6 locations is shown). Areas of significant activation are indicated as dark boxes and overlayed on baseline images (top row). Difference images reveal high intensity areas predominantly in the primary and sensorimotor cortex, and a more or less uniform noise in most other areas (bottom row). Acquisition parameters: $T_{acq}/T_E/T_R$ = 22/30/49 ms, time resolution (overall T_R) 1.76 s, flip angle 84°, 3.8 × 3.8 × 4-mm voxel size, total scan time 3 min.

TABLE 1

	Sensitivity	Image quality	Hardware demands
Multishot	Low–medium	High	Low
Single-shot	High	Low–medium	High

only gradient coils. With the advent of improved gradient hardware, this modality is becoming increasingly accessible on standard MR units.

A disadvantage of single-shot techniques is the relatively long duration of the data acquisition window. With single-shot MRI, all of k-space needs to be acquired within a single repetition (T_R), whereas with multishot techniques, k-space is populated over several T_R's. This leads to an increased sensitivity to artifacts caused by magnetic susceptibility effects, chemical shift, and T_2.

MULTISHOT MRI

Multishot MRI is less demanding on gradient hardware compared to single-shot techniques; however, this comes at the price of an increased total scan time and increased sensitivity to motion. Multishot fMRI performs several repetitions of the pulse sequence to collect the k-space data required for the image. In order to reduce the total scan time, T_R is shortened below the longitudinal relaxation time T_1 of the tissue. For optimum signal strength, partial flip angles are used [13]. An example is FLASH imaging [14–17], which acquires a single line of k-space data per T_R. Increased k-space coverage per T_R is achieved by the so-called segmented or interleaved techniques [7], which acquire multiple lines [18, 19], or a spiral interleave [20–23] per T_R (Table 1).

SCAN REQUIREMENTS FOR BOLD fMRI

Sensitivity

Changes in blood oxygenation result in changes in the apparent transverse relaxation (indicated by T_2^*), predominantly caused by microscopic susceptibility effects. At 1.5 T, the activation-related signal changes generated by this mechanism are on the order of a few percent [10]. Detection of these small changes above the fluctuations in the background signal requires a highly sensitive scan technique (i.e., a technique highly sensitive to changes in T_2^*), with an inherently high background signal stability. The latter is determined by, e.g., the signal-to-noise ratio, as well as the sensitivity to motion.

The T_2^* sensitivity is primarily determined by the acquisition parameters, the most important of which being the delay time T_E between RF excitation and the center of the data acquisition window (Fig. 1). The highest signal change with activation is found when $T_E = T_2^*$, in which T_2^* is generally in the range of 60–80 ms for gray matter at 1.5 T. The T_2^* sensitivity is less dependent on the actual acquisition technique.

On the other hand, sensitivity to, e.g., cardiac pulsations and respiratory motion results in artifacts that are dependent on acquisition parameters as well as acquisition technique. Multislice single-shot techniques are more robust in the presence of motion than 3D techniques (Fig. 3a), as are spiral scans compared to EPI [24] (Fig. 3b). To at least some extent, reduced sensitivity to motion can be accomplished by shortening T_R [22]. In cases where this requires a shortening of T_E (since $T_E < T_R$), the optimum overall fMRI scan sensitivity is found at $T_E < T_2^*$.

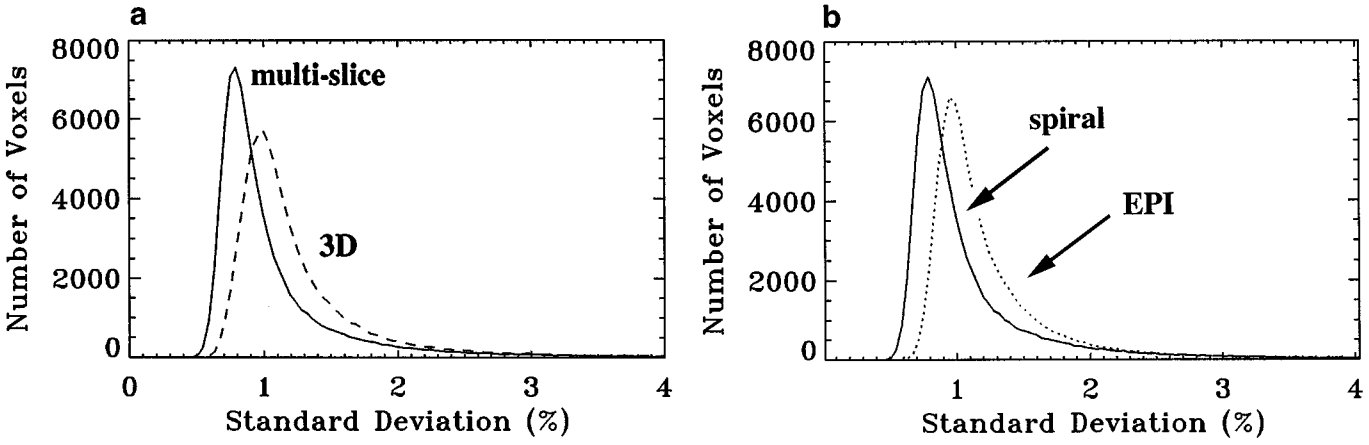

FIG. 3. Comparison of temporal stability of image intensity for baseline images with different scan techniques. Displayed are histograms of the standard deviation of the intensity, calculated on a pixel by pixel basis (averaged over nine subjects). Acquisition parameters as in Fig. 2. (a) Multislice spiral versus true 3D spiral. For the 3D experiment, a flip angle of 20° was used. The average standard deviation was 25% higher in the 3D experiments. (b) Multislice spiral versus multislice EPI. For EPI, T_R was adjusted to 55 ms to accomodate for the increased $T_{acq} = 41$ ms. 32 slices were scanned in the same overall T_R. The average standard deviation was 23% higher in the EPI experiments.

Specificity

Another important issue with fMRI is specificity; i.e., how accurately can we determine the locus of activation. The specificity is dependent on the actual image resolution, as well of the presence of image artifacts. In addition, the specificity is strongly related to the contrast mechanism responsible for the observed signal changes. The changes in signal intensity associated with BOLD contrast mechanism generally not only arise from the capillary bed, but also involve larger vessels, possibly some distance away from the activation site. The most important effects that contribute to BOLD contrast are as follows:

Inflow Effects

Inflow effects generally play an important role in single-slice 2D experiments performed under saturating conditions, i.e., when TR is not long enough to allow for substantial recovery of the longitudinal magnetization [25]. In this situation, fresh (fully recovered) spins flowing into the slice (e.g., intravascular spins) contribute more signal to the image than spins at rest. In BOLD fMRI studies, flow changes in larger vessels (>100 μm) can lead to substantial (20–30%) signal increases [26] with activation (Fig. 4) and compromise the spatial accuracy of the calculated activation map. Inflow effects are generally reduced at increased values

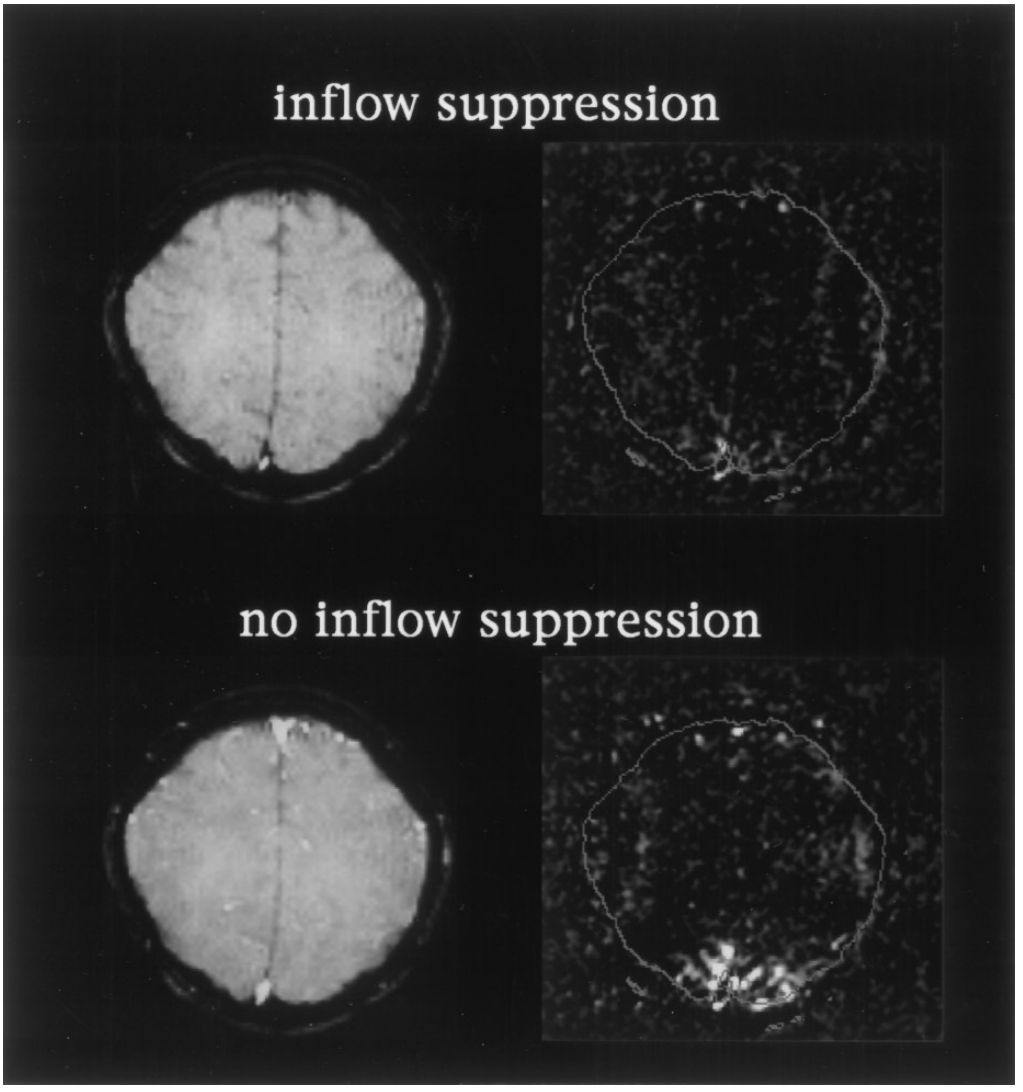

FIG. 4. Inflow effects in single-slice BOLD fMRI experiment of visual activation. An oblique axial slice through the calcarine cortex was selected. Baseline images (left) and difference images (right) with (top) and without (bottom) inflow suppression are displayed. With inflow suppression, the activation-related signal changes are reduced dramatically. Acquisition parameters: flip angle/T_E/T_R = 40°/38/60 ms, 4-mm slice thickness.

of T_R and reduced flip angles. True 3D scanning also reduces inflow effects [27], at least in the central portion of the scanned volume. With multislice 2D experiments, the contribution of inflow effects to the activation-related signal change is very much dependent on experimental parameters, and blood flow velocity, and can result in positive, as well as negative, signal changes with activation (Fig. 5).

Macroscopic (Bulk) Susceptibility Effects

The representation of BOLD susceptibility effects by a monoexponential signal decay over time is only valid in a volume element (voxel) with a large number of randomly oriented capillaries [28–30], as possibly is the case in some parts of the brain parenchyma. The validity of this model in the general case is questionable, as there are likely to be many image voxels containing vessels significantly larger than the average capillary size (2–5 μm), for which the assumption of random distribution of orientations does not hold. Single-vessel models [31] point to significant activation-related signal changes due to interference of intra- and extravascular magnetization, as well as due to interference of multiphase extravascular signals. Under certain conditions, up to 12% signal changes can be expected for vessels occupying only 4% of the voxel [31].

Signal Changes during Acquisition

Signal changes during the acquisition window can lead to image artifacts, especially when a long acquisition window is used (e.g., with single-shot techniques). In addition to T_2^*-related signal decay, bulk susceptibility effects in or around larger vessels can lead to signal phase and amplitude changes during the acquisition window. With EPI and spiral imaging, such changes can lead to shifting of signal intensity in the image, reducing the accuracy of the activation image (Fig. 6a). Experimental visualization of this effect can be facilitated with bolus-tracking studies with exogenous susceptibility contrast agents, in which intra- and perivascular frequency shifts are several times higher than encountered with BOLD fMRI studies (Fig. 6b).

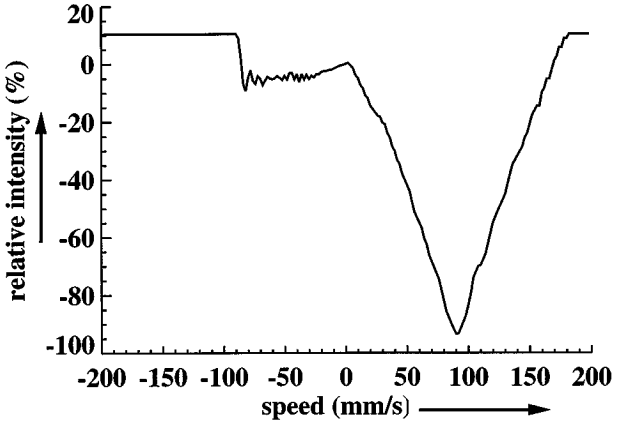

FIG. 5. Calculated flow-related signal change for spins moving perpendicularly to image plane. The rest magnetization in the central slice in a sequential multislice experiment for spins moving with the scan direction (positive velocities) and against the scan direction (negative velocities) was simulated. Note the large signal loss for spins moving at the same speed as the scan speed (89 mm/s). Other parameters used in the simulation: flip angle/T_R = 84°/1800 ms, 4-mm slice thickness, 40 slices.

Anatomical Coverage

For most applications of fMRI, it is important to scan a relatively large part of the brain, either by a slice by slice (multislice) protocol or by a true 3D acquisition. Both allow coverage of most of the brain within a few seconds. In a 3D acquisition, 3D k-space data are collected over multiple repetitions, and signal modulations related to motion (e.g., CSF pulsations, related to cardiac and/or respiratory cycle) affect the entire volume. The lack of single-shot 3D techniques, resulting in a relatively long scan duration, renders 3D acquisition susceptible to motion-related artifacts, e.g., a reduced scan-to-scan stability (Fig. 3a). Therefore, the advantage of a reduced contribution of inflow effects with 3D scans [31] comes at the price of a lower overall sensitivity.

SCAN OPTIONS

RF Phase Spoiling

MRI experiments with T_R well below the tissue T_2 values, e.g., true 3D experiments, are generally sensitive to motion of those spins [32–34]. In this situation, patient motion can lead to fluctuation in signal intensity over time. Techniques that employ RF phase spoiling [35] have reduced sensitivity to motion (Fig. 7). The observed improvement in signal stability is dependent on the RF phase modulation scheme, as well as on T_R and flip angle [36].

Echo Shifting

Echo shifting [37, 31] enables scanning with $T_E > T_R$, by using pulsed gradients flanking the RF excitation to delay the signal beyond a subsequent excitation. This allows shortening of T_R, and a reduction of the "dead time" between excitation and acquisition, thereby reducing the total measurement time. The potential advantage of this scheme for fMRI is twofold: it allows increased signal averaging at a fixed scan time, as well as reduced sensitivity to motion related to shortening of T_R [22].

Unfortunately, in practice, this does not necessarily translate into an improvement in overall sensitivity.

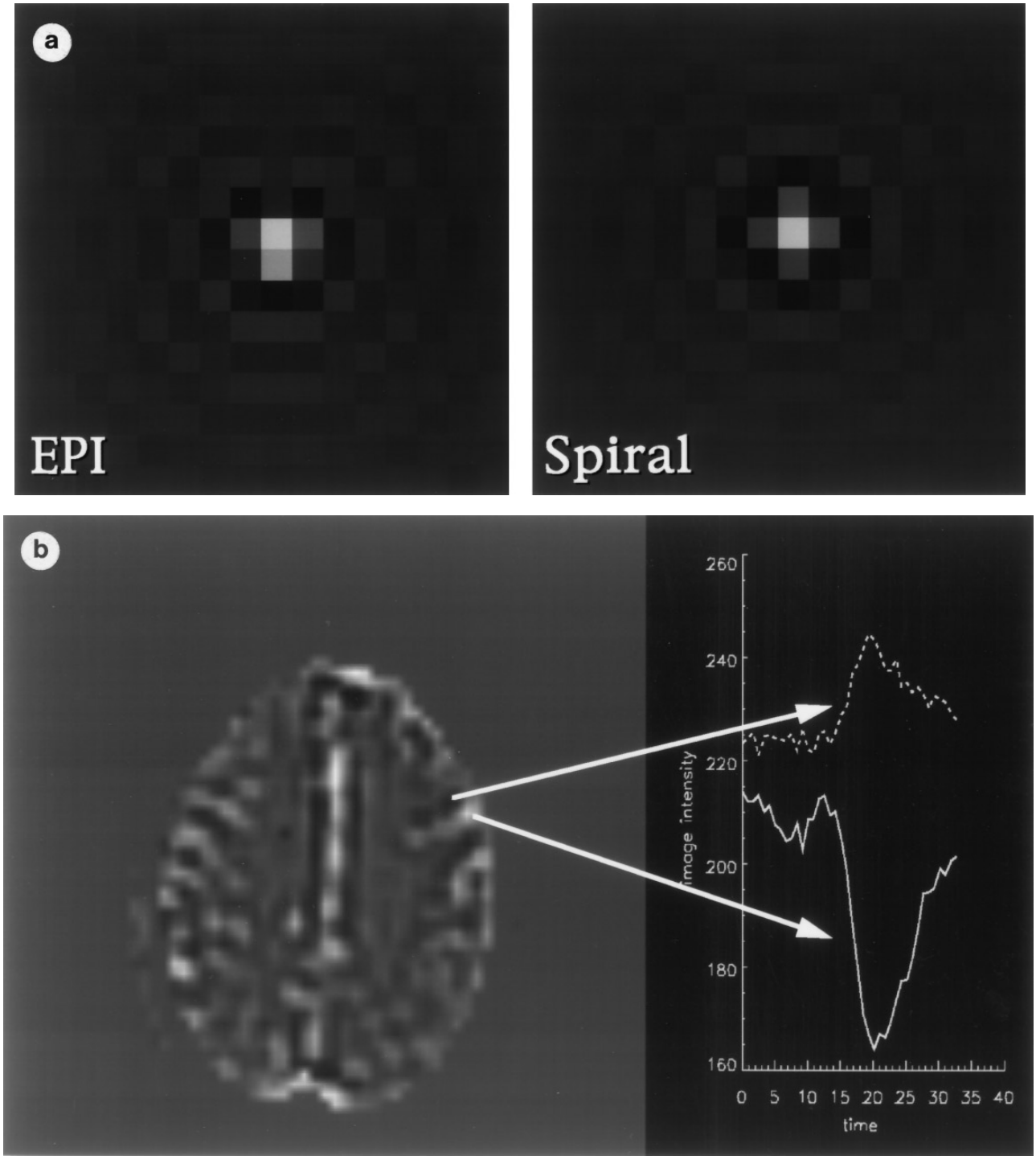

FIG. 6. Off-resonance effects in spiral and EPI fMRI. (a) Calculated effect of off-resonance in EPI and spiral fMRI, assuming a single vessel in one voxel, parallel with the magnetic field, and occupying 10% of the voxel volume. In both EPI and spiral difference images, the activation-related frequency shift inside the vessel leads to an intensity increase in the pixel containing the vessel. The frequency shift affects surrounding pixels as well, and in some pixels leads to intensity decrease. Qualitatively similar effects were observed for vessels running perpendicular to the magnetic field. Parameters: $T_E = T_{acq} = 40$ ms, blood oxygenation levels 0.55 (rest state) and 0.7 (activated state), 40% hematocrit, 1.5 T main field. (b) Bolus-tracking experiment with spiral scan. The experiment was performed with $T_{acq}/T_E/T_R = 22/17/35$ ms, flip angle 50°, 24 × 4-mm-thick slices, time resolution (overall T_R) 840 ms, 0.15 mmol/kg intravenous injection of Gd-DTPA. The short T_E (relative to T_{acq}) was chosen to sensitize to effects of T_{acq}. The reconstructed blood volume map (obtained from curve fitting of the time-course data) shows dark bands surrounding bright areas, indicating signal increase with passage of the bolus of paramagnetic contrast agent. The effect is attributed to an intra- and perivascular frequency shift associated with the contrast agent.

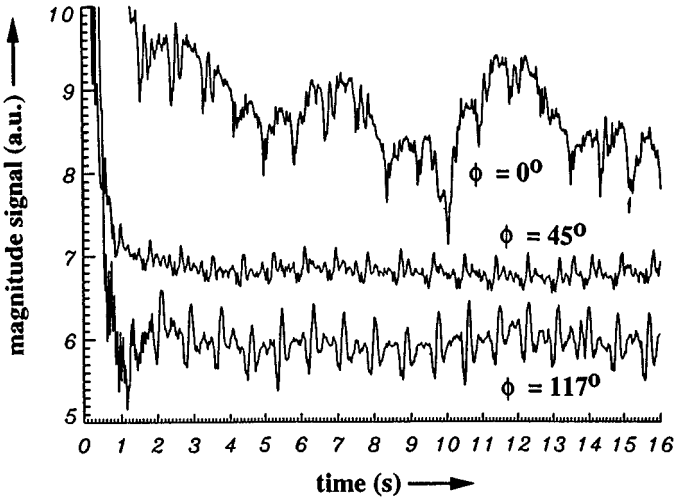

FIG. 7. Effect of RF phase spoiling on signal stability in single slice experiment (no activation). Repeated scanning was performed with T_R = 40 ms and a flip angle of 40°. Quadratic RF phase modulation was performed with $f = 0°$ (no spoiling), $f = 117°$, and $f = 45°$. Offsets of −0.5, 0, and +1, respectively, were added to the data to separate the signals. Note the reduction of fluctuations related to heartbeat and respiratory cycle at $f = 45°$.

This has the following reasons: (1) The RF flip angle, as well as the signal strength are reduced with shortening of T_R and (2) the use of additional gradient pulses leads to increased sensitivity to motion. The net effect of echo shifting on sensitivity depends on the experimental parameters, but oftentimes is small or even negative. Figure 8 shows the result of echo shifting on the background signal stability in a multislice spiral fMRI experiment. A slight reduction in stability is observed with echo shifting. With true 3D scanning, a larger reduction in stability was observed.

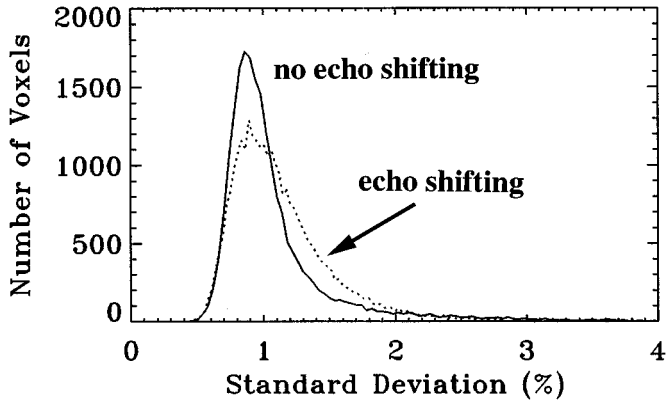

FIG. 8. Comparison of temporal stability of image intensity for baseline multislice spiral images with echo shifting and without echo shifting, presented as a histogram of the standard deviation of the intensity (calculated on a pixel by pixel basis). T_{acq}/T_E was 22/51 ms, T_R/flip angle was 35 ms/15° and 70 ms/21° for echo shifting and no echo shifting, respectively. The voxel size was 3.8 × 3.8 × 4 mm. For echo shifting, the standard deviation was corrected for the reduction in scan time. Note the slight increase in standard deviation with echo shifting.

Spin Echo fMRI

In MRI, part of the signal loss related to susceptibility effects can be recovered by using a so-called "spin-echo" sequence, which uses an additional RF pulse (also called refocusing or 180° pulse). With appropriate positioning of this pulse, most of the phase dispersal (differences in phase accumulation) between the spins is eliminated at time T_E. The spin echo signal decay is characterized by T_2 (as opposed to T_2^*). Also the spin echo signal is sensitive to blood oxygenation changes, with a contrast mechanism believed to originate predominantly in tissue surrounding the capillaries [38, 39], whereas the relative contribution of larger vessels is small. T_2-weighted fMRI would therefore more specifically localize the neuronal activity. A disadvantage of the spin echo sequence is the reduced sensitivity, and the fact that pure T_2 sensitivity is only reached at time T_E (peak of the echo). Techniques that use T_{acq} of substantial duration (e.g., similar to or longer than the echo time T_E) are therefore also sensitive to T_2^* (as well as bulk susceptibility effects) and can therefore have significant signal contributions originating from larger vessels.

CONCLUSION

Recent improvements in scanner hardware have allowed a more widespread use of single-shot MR scan techniques for fMRI. Coverage of the entire brain with high sensitivity is currently achievable with temporal resolutions of around 2 s. To minimize image artifacts, the duration of the data acquisition windows needs to be kept at minimum.

ACKNOWLEDGMENTS

Gary H. Glover and Marc Alley (Stanford University), as well as Peter van Gelderen and Danny Weinberger (NIH), are acknowledged for their support in the development of the spiral MR techniques.

REFERENCES

1. Williams, D. S., Detre, J. A., Leigh, J. S., and Koretsky, A. P. 1992. Magnetic resonance imaging of perfusion using spin inversion of arterial water. *Proc. Natl. Acad. Sci. USA* **89:**212–216.
2. Rosen, B. R., Belliveau, J. W., Vevea, J. M., and Brady, T. J. 1990. Perfusion imaging with NMR contrast agents. *Magn. Reson. Med.* **14:**249–265.
3. Belliveau, J. W., Kennedy, D. N., McKinstry, R. C., Buchbinder, B. R., Weisskoff, R. M., Cohen, M. S., Vevea, J. M., Brady, T. J., and Rosen, B. R. 1991. Functional mapping of the human visual cortex by magnetic resonance imaging. *Science* **254:**716–719.
4. Ogawa, S., Lee, T. M., Nayak, A. S., and Glynn, P. 1990. Oxygenation-sensitive contrast in magnetic resonance imaging

of rodent brain at high magnetic fields. *Magn. Reson. Med.* **14:**68–78.

5. Ogawa, S., Lee, T. M., Ray, A. R., and Tank, D. W. 1990. Brain magnetic resonance imaging with contrast dependent on blood oxygenation. *Proc. Natl. Acad. Sci. USA* **87:**9868–9872.
6. Lauterbur, P. C., Kramer, D. N., House, W. V., and Chen, C. N. 1975. Zeugmatographic high resolution nuclear magnetic resonance spectroscopy: Images of chemical inhomogeneity within macroscopic objects. *J. Am. Chem. Soc.* **97:**6866.
7. Likes, R. S. 1981. Moving gradient zeugmatography. U.S. Patent 4307343.
8. Twieg, D. B. 1983. The k-trajectory formulation of the NMR imaging process with applications in analysis and synthesis of imaging methods. *Med. Phys.* **10:**610–621.
9. Mansfield, P., and Pykett, I. 1978. Biological and medical imaging by NMR. *J. Magn. Reson.* **29:**355–373.
10. Kwong, K. K., Belliveau, J. W., Chesler, D. A., Goldberg, I. E., Weiskoff, R. M., Poncelet, B. P., Kennedy, D. N., Hoppel, B. E., Cohen, M. S., Turner, R., Cheng, H., Brady, T. J., and Rosen, B. R. 1992. Dynamic magnetic resonance imaging of human brain activity during primary sensory stimulation. *Proc. Natl Acad. Sci. USA* **89:**5675–5679.
11. Bandettini, P. A., Wong, E. C., Hinks, R. S., Tikofsky, R. S., and Hyde, J. S. 1992. Time course EPI of human brain function during task activation. *Magn. Reson. Med.* **25:**390–397.
12. Meyer, C. H., Hu, B. S., Nishimura, D. G., and Macovski, A. 1992. Fast spiral coronary artery imaging. *Magn. Reson. Med.* **28:**202–213.
13. Ernst, R. R., and Anderson, W. A. 1966. Application of Fourier transformation spectroscopy to magnetic resonance. *Rev. Sci. Instr.* **37:**93–102.
14. Haase, A., Frahm, J., Matthaei, D., Haenicke, W., and Merboldt, K. D. 1986. Flash imaging: Rapid NMR imaging using low flip angle pulses. *J. Magn. Reson.* **67:**217–225.
15. Ogawa, S., Tank, D. W., Menon, R., Ellermann, J. M., Kim, S. G., Merkle, H., and Ugurbil, K. 1992. Intrinsic signal changes accompanying sensory stimulation: Functional brain mapping with magnetic resonance imaging. *Proc. Natl. Acad. Sci. USA* **89:**5951–5955.
16. Frahm, J., Bruhn, H., Merboldt, K. D., and Hanicke, W. 1992. Dynamic MR imaging of human brain oxygenation during rest and photic stimulation. *J. Magn. Reson. Imag.* **2:**501–505.
17. Kim, S. G., Ashe, J., Georgopoulos, A. P., Merkle, H., Ellermann, J. M., Menon, R. S., Ogawa, S., and Ugurbil, K. 1993. Functional imaging of human motor cortex at high magnetic field. *J. Neurophysiol.* **69:**297–302.
18. van Uijen, C. M. J., den Boef, J. H., and Verschuren, F. J. J. 1985. Fast Fourier imaging. *Magn. Reson. Med.* **2:**203–217.
19. van Gelderen, P., Ramsey, N. F., Liu, G., Duyn, J. H., Frank, J. A., Weinberger, D. R., and Moonen, C. T. W. 1995. Three-dimensional functional magnetic resonance imaging of human brain on a clinical 1.5-T scanner. *Proc. Natl. Acad. Sci. USA* **92:**6906–6910.
20. Meyer, C. H., and Macovski, A. 1987. Square spiral fast imaging: Interleaving and off-resonance effects. In *Proceedings, 6th Annual Meeting, Society of Magnetic Resonance in Medicine*, p. 230, SMRM1987:230.
21. Noll, D. C., Cohen, J. D., Meyer, C. H., and Schneider, W. 1995. Spiral k-space MR imaging of cortical activation. *J. Magn. Reson. Imag.* **5:**49–56.
22. Glover, G. H., and Lee, A. T. 1995. Motion artifacts in fMRI: Comparison of 2DFT with PR and spiral scan methods. *Magn. Reson. Med.* **33:**624–635.
23. Yang, Y., Glover, G. H., van Gelderen, P., Mattay, V. S., Santha, A. K. S., Sexton, R. H., Ramsey, N. R., Moonen, C. T. W., Weinberger, D. R., Frank, J. A., and Duyn, J. H. 1996. 3D functional magnetic resonance imaging at 1.5 T with spiral acquisition. *Magn. Reson. Med.* **36:**620–626.
24. Nishimura, D. G., Irarrazabal, P., and Meyer, C. H. 1995. A velocity k-space analysis of flow effects in echo-planar and spiral imaging. *Magn. Reson. Med.* **33:**549–556.
25. Gao, J. H., Holland, S. K., and Gore, J. C. 1988. Nuclear magnetic resonance signal from nuclei in rapid imaging using gradient echoes. *Med. Phys.* **15:**809–814.
26. Duyn, J. H., Moonen, C. T. W., van Yperen, G. H., de Boer, R. W., and Luyten, P. R. 1994. Inflow versus deoxyhemoglobin effects in 'BOLD' functional MRI using gradient echoes at 1.5 T. *NMR Biomed.* **7:**83–88.
27. Duyn, J. H., Mattay, V. S., Sexton, R. H., Sobering, G. S., Barrios, F. A., Liu, G., Frank, J. A., Weinberger, D. R., and Moonen, C. T. W. 1994. 3-dimensional functional imaging of human brain using echo-shifted FLASH MRI. *Magn. Reson. Med.* **32:**150–155.
28. Ogawa, S., Menon, R., Tank, D., Kim, S. G., Merkle, H., Ellerman, J. M., and Ugurbil, K. 1993. Functional brain mapping by blood oxygenation dependent contrast magnetic resonance imaging: A comparison of signal characteristics with a biophysical model. *Biophys. J.* **64:**803–812.
29. Weisskoff, R. M., Zuo, C. S., Boxerman, J. L., and Rosen, B. R. 1994. Microscopic susceptibility variation and transverse relaxation: Theory and experiment. *Magn. Reson. Med.* **31:**601–610.
30. Kennan, R. P., Zhong, J., and Gore, J. C. 1994. Intravascular susceptibility contrast mechanisms in tissues. *Magn. Reson. Med.* **31:**9–21.
31. Lai, S., Hopkins, A. L., Haacke, E. M., Li, D., Wasserman, B. A., Buckley, P., Friedman, L., Metzler, A., Hedera, P., and Friedland, R. 1993. Identification of vascular structures as a major source of signal contrast in high resolution 2D and 3D functional activation imaging of motor cortex at 1.5 T: Preliminary results. *Magn. Reson. Med.* **30:**387–392.
32. Patz, S., and Hawkes, R. C. 1986. The application of steady-state free precession to the study of very slow fluid flow. *Magn. Reson. Med.* **3:**140–145.
33. Haacke, E. M., Wielopolski, P. A., Tkach, J. A., and Modic, M. T. 1990. Steady-state free precession imaging in the presence of motion: Application for improved visualization of the cerebrospinal fluid. *Radiology* **175:**545–552.
34. Merboldt, K. D., Frahm, J., Gyngell, M. L., Haenicke, W., and Deimling, M. 1989. MRI of diffusion in the human brain: New results using a modified CE-FAST sequence. *Magn. Reson. Med.* **9:**423–429.
35. Zur, Y., Wood, M. L., and Neuringer, L. J. 1991. Spoiling of transverse magnetization in steady-state sequences. *Magn. Reson. Med.* **21:**251–263.
36. Duyn, J. H. 1996. Steady state effects in fast gradient echo imaging. *Magn. Reson. Med.*, in press.
37. Moonen, C. T. W., Liu, G., van Gelderen, P., and Sobering, G. 1992. A fast gradient-recalled MRI technique with increased sensitivity to dynamic susceptibility effects. *Magn. Reson. Med.* **26:**184–189.
38. Constable, R. T., Kennan, R. P., Puce, A., McCarthy, G., and Gore, J. C. 1994. Functional NMR imaging using fast spin echo at 1.5 T. *Magn. Reson. Med.* **31:**686–690.
39. Bandettini, P. A., Wong, E. C., Jesmanowicz, A., Hinks, R. S., and Hyde, J. S. 1994. Spin-echo and gradient-echo EPI of human brain activation using BOLD contrast: A comparative study at 1.5 T. *NMR Biomed.* **7:**12–20.